doi:10.1016/j.jmb.2007.04.082 J. Mol. Biol. (2007) 371, 396–409

JMB

Available online at www.sciencedirect.com

ScienceDirect

ELSEVIER

pH Modulates the Quinone Position in the Photosynthetic Reaction Center from *Rhodobacter sphaeroides* in the Neutral and Charge Separated States

Juergen Koepke[1]*, Eva-Maria Krammer[2], Astrid R. Klingen[2] Pierre Sebban[3], G. Matthias Ullmann[2] and Günter Fritzsch[1]

[1]*Max Planck Institute of Biophysics, Department of Molecular Membrane Biology Max-von-Laue Straße 3 D-60438 Frankfurt/Main Germany*

[2]*Structural Biology/ Bioinformatics, University of Bayreuth, Universitätsstr. 30 BGI, 95447 Bayreuth, Germany*

[3]*Laboratoire de Chimie-Physique, UMR 8000 Université Paris XI/CNRS Bât. 350 91405 Cedex Orsay, France*

**Corresponding author*

The structure of the photosynthetic reaction-center from *Rhodobacter sphaeroides* has been determined at four different pH values (6.5, 8.0, 9.0, 10.0) in the neutral and in charge separated states. At pH 8.0, in the neutral state, we obtain a resolution of 1.87 Å, which is the best ever reported for the bacterial reaction center protein. Our crystallographic data confirm the existence of two different binding positions of the secondary quinone (Q_B). We observe a new orientation of Q_B in its distal position, which shows no ring-flip compared to the orientation in the proximal position. Datasets collected for the different pH values show a pH-dependence of the population of the proximal position. The new orientation of Q_B in the distal position and the pH-dependence could be confirmed by continuum electrostatics calculations. Our calculations are in agreement with the experimentally observed proton uptake upon charge separation. The high resolution of our crystallographic data allows us to identify new water molecules and external residues being involved in two previously described hydrogen bond proton channels. These extended proton-transfer pathways, ending at either of the two oxo-groups of Q_B in its proximal position, provide additional evidence that ring-flipping is not required for complete protonation of Q_B upon reduction.

Keywords: X-ray crystallography; pH-value; proton-uptake; secondary quinine; proton-transfer pathways

Introduction

The bacterial photosynthetic reaction center (RC) is a membrane-spanning protein complex, which converts light energy into chemical free energy. The photosynthetic RC of *Rhodobacter sphaeroides (Rb. sphaeroides)* consists of three protein subunits L, M, and H. The L and M subunits, each contain five membrane-spanning helices. Together they bind non-covalently the ten cofactors. The H subunit has only one helical membrane anchor. The system is 2-fold pseudo-symmetric; the symmetry axis runs from a dimer of bacteriochlorophyll molecules (P), located on the periplasmic side of the complex, to a non-heme iron atom situated between the primary quinone (Q_A) and the secondary quinone (Q_B), close to the cytoplasmic side of the complex. Light energy is trapped by the primary electron donor P. The absorption of a photon generates the exited electronic singlet state of lowest energy of P, the excited dimer (P*), which is a strongly reducing species. Transmembrane electron transfer is then initiated from P* to the system of two quinones, Q_A and Q_B, bound at the cytoplasmic side of the RC. Q_A and Q_B differ in their redox properties. Q_A is never protonated and accepts only one electron. Q_B (the terminal electron acceptor) sequentially accepts two

Abbreviations used: RC, reaction center; PDB, Protein Data Bank; PC, phosphatidylcholine; GGD, glucosylgalactosyl diacylglycerol; LDAO, lauryldimethylamine *N*-oxide.

E-mail address of the corresponding author: Juergen.Koepke@mpibp-frankfurt.mpg.de

electrons and two protons to form the dihydroquinone species (Q_BH_2). The latter species is released from the RC to deliver its reducing power to the bc_1 complex and is replaced by an oxidized ubiquinone from the quinone pool present in the membrane.

Q_A is tightly bound to the complex in contrast to Q_B, which is firmly bound in the semiquinone state but is loosely attached in the neutral forms Q_B and Q_BH_2. Different positions of Q_B depending on the redox state of the protein have initially been discussed by Stowell *et al*.[1] Based on crystallographic data, these authors found that Q_B could be located either in a so-called distal position in the dark-adapted state of the RC (Q_B oxidized) or in a proximal position in the illuminated state (Q_B singly reduced). Distal and proximal refer to the Q_B position relative to the non-heme iron. Q_B was proposed to undergo a light-induced shift of ~4.5 Å towards the non-heme iron, accompanied by a 180° propeller twist around the isoprenoid tail.[1] More recent crystallographic investigations showed Q_B electron density both in the distal and proximal positions of Q_B in the dark as well as under illumination.[2]

A direct correspondence between the two positions of Q_B and its redox states, as well as movement of Q_B between the two positions being rate-limiting for electron transfer to Q_B[3,4] is nowadays considered as unlikely.[5,6] Moreover, a recent molecular dynamics study[7] comes to the conclusion, that the distal Q_B position found in published RC X-ray structures can be interpreted as unproductive. However, it is of interest to understand why Q_B may occupy two positions and what are the energetic parameters that govern the relative population of the different positions.

A theoretical analysis of proton uptake upon Q_B reduction recently suggested a dependence of the Q_B position on pH.[8] To investigate this suggested pH dependence, we have determined the structures of the RC at four different pH values, both in the dark-adapted and the illuminated state. The electron density of the distal position is best fitted by an orientation of Q_B, which is similar to its orientation in the proximal position. Our orientation of Q_B in the distal position thus differs from the previously proposed orientation.[1] Although, the electrostatic calculations of this work show only little energetic difference between the previous and our new distal Q_B orientation, the movement of Q_B between the distal and the proximal position seems easily possible without requiring a rotation of the whole Q_B by 180° inside the binding pocket. Thus, with our new distal Q_B orientation, a propeller twist around the isoprenoid tail of Q_B is not required for the movement of the ubiquinone from the distal to the proximal position. Using the new orientation of Q_B in the distal position, we have calculated the population of the Q_B positions and quantified proton uptake upon semiquinone formation of Q_B. Our data indicate that pH is a factor in modulating the quinone position and the associated proton uptake.

Results and Discussions

Structural basis and general features of the high resolution structure

Here, we have investigated the structure of the photosynthetic RC from *Rb. sphaeroides* at liquid nitrogen temperature. Since the resolution especially for the data collected in the dark at a pH of 8 could be considerably improved compared to the structure determined at 277 K[9] (PDB data base entry 1pcr), the number of modeled water molecules that could be included in to the model increased from 160 to 430. For the cryo-cooled structure, several new water molecules are visible in the membrane spanning part of the RC. These water molecules constitute two hydrogen-bonded networks between Q_B and the bulk solvent at the cytoplasmic side of the RC, including several charged residues and the ligands of the non-heme iron. These two water chains confirmed by our work have been described before.[1,9] Two water molecules of the 277 K structure at the Q_B side of the water chains (Wat65 and 66 of 1pcr) are replaced by Q_B in the proximal position of the cryo-cooled structure of this work. Furthermore, we could confirm previous Raman and NMR spectroscopic results[10,11] concerning the kinked conformation of the carotenoid molecule and indicating a 15,15′-*cis* bond in all our refinements. Such a conformation has also been proposed in *Rhodopseudomonas viridis* RC.[12] Two of the three refined lipid molecules, glucosylgalactosyl diacylglycerol (GGD) and phosphatidylcholine (PC), had to be oriented differently compared to those of Camara-Artigas *et al*.,[13] to fit the available electron density (Figure 1). This re-orientation abandons the unusual conformations described previously[13] and places the head-groups of these lipids in an orientation pointing towards the water molecules above the cytoplasmic surface (Figure 1(d)). In addition, the conflict in positioning of both the PC and the isoprenoid tail of Q_B in the distal position is abolished (Figure 1(c)). The density for the lipid hydrocarbon chains, that was occupied by four lauryldimethylamine *N*-oxide (LDAO) detergent molecules in other structures, is very distinct, but the density for the head-groups is not very pronounced, which could lead to misinterpretation.[14]

Binding of Q_B

The orientation of Q_B in the proximal and distal position cannot be determined unambiguously from the electron density. For the proximal position, only the positioning of the two oxo-groups of Q_B between the hydrogen bond partners His L190 $N^{\delta 1}$ and Gly L225 N and the position of one methoxy-group, which accepts a weaker hydrogen bond from Thr L226 N, seems to be secure. These restraints still allow two possible orientations of Q_B in the proximal position, which are related to each other by an approximately 180° rotation around the longitudinal pseudo-symmetry axis of the head-group ring of Q_B,

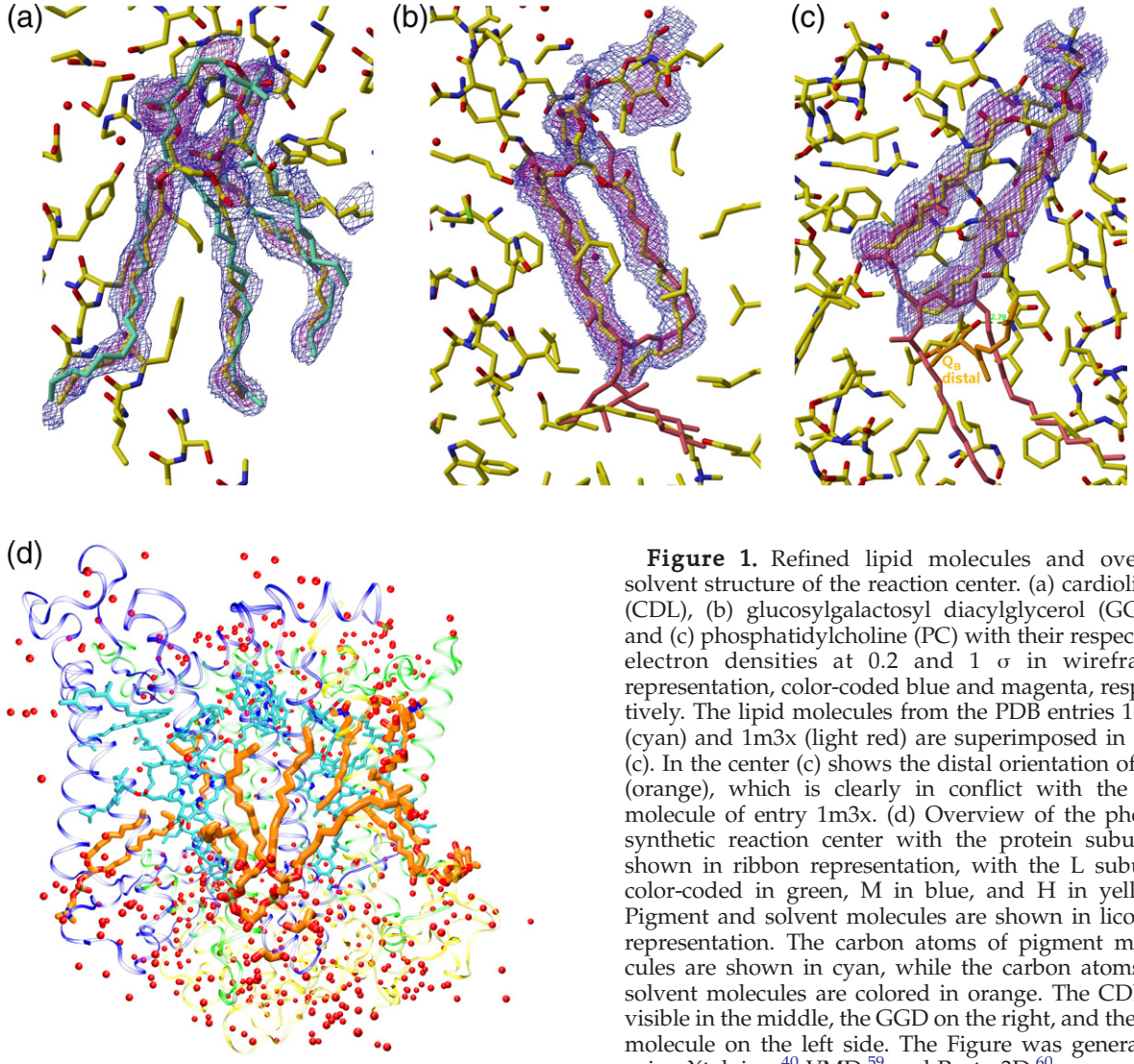

Figure 1. Refined lipid molecules and overall solvent structure of the reaction center. (a) cardiolipin (CDL), (b) glucosylgalactosyl diacylglycerol (GGD), and (c) phosphatidylcholine (PC) with their respective electron densities at 0.2 and 1 σ in wireframe representation, color-coded blue and magenta, respectively. The lipid molecules from the PDB entries 1qov (cyan) and 1m3x (light red) are superimposed in (a)–(c). In the center (c) shows the distal orientation of Q_B (orange), which is clearly in conflict with the PC molecule of entry 1m3x. (d) Overview of the photosynthetic reaction center with the protein subunits shown in ribbon representation, with the L subunit color-coded in green, M in blue, and H in yellow. Pigment and solvent molecules are shown in licorice representation. The carbon atoms of pigment molecules are shown in cyan, while the carbon atoms of solvent molecules are colored in orange. The CDL is visible in the middle, the GGD on the right, and the PC molecule on the left side. The Figure was generated using Xtalview,[40] VMD,[59] and Raster3D.[60]

leading to two different orientations of the isoprenoid tail. A fit to the shorter electron density rod extending from the head group density was chosen for our model (Figure 2(a)). The resulting orientation is roughly in agreement with that in the illuminated structure of Q_B (PDB entry 1aij) found by Stowell *et al.*[1] as may be seen in Figure 2(b). The distal position of Q_B is restrained by only a single hydrogen bond between one oxo-group of Q_B and the N of Ile L224. The electron density again gives no clear information about the orientation of Q_B in this position. Two weak (about 0.2 σ) electron density rods extend from the head-group density; each of them can accommodate the isoprenoid tail leading again to two possible Q_B orientations (Figure 2(a)). The longer of these density rods was used to model the distal isoprenoid tail, leading to a Q_B orientation that differs from previous models.[1] The corresponding density here was interpreted as a PC molecule. The new orientation of Q_B in the distal position allows a movement to the proximal position without the so-called propeller twist around the longitudinal pseudo-symmetry axis of the head-group ring. To analyze the relative energetics of the two orientations in the distal position, we performed quantum chemical and electrostatic calculations. The quantum chemical calculations using density functional theory show that the two possible orientations of isolated Q_B are energetically close: the non-ring-flipped orientation of the isolated Q_B is favored by 0.4 kcal/mol. Also the electrostatic interaction of the protein with Q_B allows both orientations with approximately equal energy.

From our Monte Carlo simulations, we estimate that electrostatic contributions to the difference between the ring-flipped and the non-ring-flipped orientation range from 0.3 kcal/mol at pH 6 to 0.0 kcal/mol at pH 10, favoring the non-flipped orientation.

Movement of Q_B

The present, high resolved crystallographic information allows us to propose a mechanism for the movement of Q_B between its two putative positions.

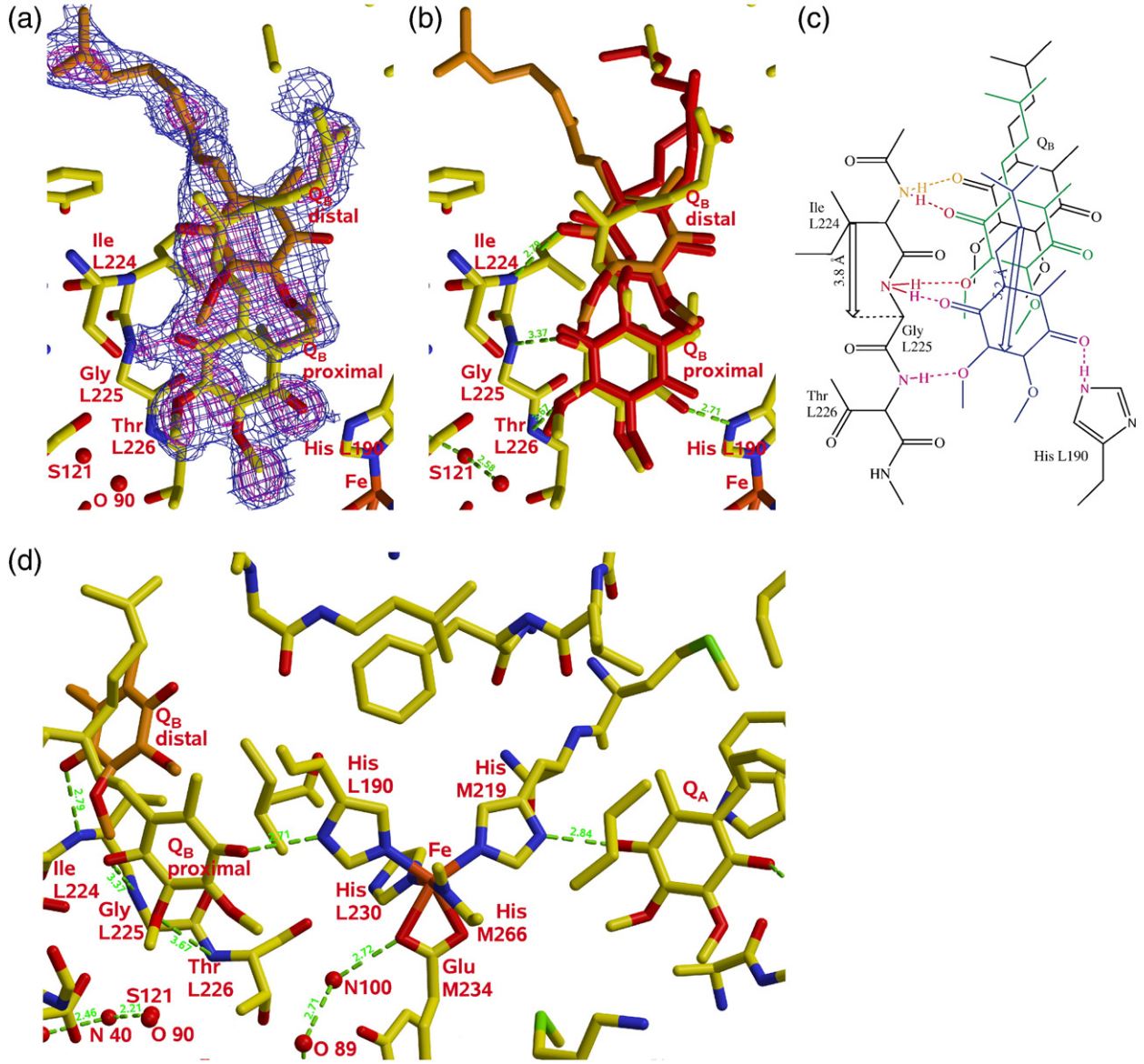

Figure 2. (a) Electron density around the distal and proximal Q_B positions in the structure of this work (pH 8, dark-adapted state; PDB entry 2j8c). The 0.2 and the 1σ levels of the density are depicted in blue and magenta wireframes, respectively. The models for the distal (orange) and the proximal (yellow) positions are shown as stick model. The two head-groups are tilted out of the image plane by about ±15°. (b) Superposition of the two Q_B positions, color-coded in yellow, orange, and red, respectively, with the structures from Stowell *et al.*[1] (PDB entries 1aig and 1aij) of the same state and at the same pH, shown in red. Hydrogen bonds to neighboring protein atoms are indicated by broken green lines, with their length given in Å. (c) Schematic drawing of the Q_B movement. Distal position in black, hypothetical intermediate position in green, and proximal Q_B position in blue. Hydrogen bonds to the distal position are color-coded orange, to the intermediate position in red, and to the proximal Q_B position in magenta. The length of the total Q_B movement and the C^{α}–C^{α} distance are indicated by arrows. (d) View onto the two quinone binding sites of Q_A and Q_B demonstrating the approximate 2-fold symmetry between Q_A and the proximal Q_B position (yellow), relative to an axis from the special pair (not visible) to the none-heme iron labeled Fe. The central none-heme iron is coordinated by four histidine residues (L190, L230, M219, and M266) and a glutamic acid (M234). Possible hydrogen bonds are indicated by broken green lines, with their length given in Å. Xtalview[40] was used for visualization, Raster3D[60] for rendering, and ChemDraw for the schematic drawing.

The distal position is only weakly stabilized by a single hydrogen bond between Q_B and Ile L224 N (Figure 2(c)). An intermediate position with two hydrogen bonds of the protein towards one oxo and one methoxy-group on the same side of Q_B, might be conceivable when Q_B moves from the distal to the proximal position (Figure 2(c)). Q_B could glide along the backbone from Ile L224 towards Gly L225, keeping thereby the contact to Ile L224 N and forming a new one to Gly L225 N. Unfortunately, is it not possible to unambiguously determine such an intermediate position from the electron density. The distance of the final movement from this hypothetical intermediate with its two hydrogen bonds

towards the proximal position is then about 3.8 Å, corresponding to the C^{α}–C^{α} distance between two residues. Not only does the oxo-group of Q_B bind to the new hydrogen bond partner Gly L225 N on its way deeper into the pocket, but also the Q_B is able to move further until the methoxy-group on the same side of Q_B is in hydrogen bond distance to the adjacent backbone nitrogen Thr L226 N. In this position, the other oxo-group of Q_B is in hydrogen bond distance to His L190 $N^{\delta 1}$ and three H-bonds are formed (Figure 2(c)) between the protein and Q_B with a geometry symmetric to Q_A (Figure 2(d)). The total movement of Q_B is therefore with 5.2 Å longer than the C^{α}–C^{α} distance and the overall movement thus gradually increases the number of H-bonds accepted by Q_B from one to three.

Proton delivery to Q_B

Two proton uptake pathways from the cytoplasm to Q_B and ending either close to Glu L212 or Asp L213, respectively, have previously been identified[1,9,15] (defined below as E- and D-pathways according to these two residues). Glu L212 and Asp L213 have been suggested to be the ultimate carriers of the first[16] and the second proton, respectively,[17] to Q_B. The improved resolution of our crystallographic data allows us to observe extensions of these pathways including the participation of new water molecules and new external residues (see below).

Glu L212 itself is in hydrogen bond distance to Wat O89 of the E-pathway water chain (Figure 3(a) and (c)) and in close distance to one methoxy-oxygen of Q_B in the proximal position (3.5 Å). Water molecule N100 connects the E-pathway *via* two H-bonds to Glu M234, coordinating the none-heme iron. The D-pathway water chain (Figure 3(b) and (d)) extends directly to the vicinity of the second methoxy-group, with the water molecules O90, N40, and N39 hydrogen-bonded to Asp L213. Both pathways have no direct connection to the bulk solvent in our structure, but start at Arg H118 (E-pathway) or Arg M13 (D-pathway). Arg H118 was found in two orientations, indicating the flexibility of these two arginine residues, which could allow proton uptake from the bulk solvent to the water chains by a spatial movement. At the entry of the E-pathway, also Asp M240 might be responsible for proton translocation, but the Arg H118 seems more likely to be involved, due to its obvious flexibility. These two pathways probably each deliver a proton to either side of Q_B after its reduction. We do not see a direct connection of the two pathways to the two Q_B oxo-groups, therefore two additional mobile water molecules, not visible to the X-ray experiment, might be required for the protonation of the Q_B oxo-groups (indicated in Figure 3(c) and (d) by a hypothetical, flexible water molecule). Due to the existence of the two separate proton pathways, proton uptake by the two oxo-groups of Q_B does not require rotation of Q_B.

Both the new and the old Q_B orientations seem to differ energetically only slightly from structural and theoretical considerations, but only in the new Q_B orientation a movement between the proximal and the distal Q_B positions seems to be possible without large conformational rearrangements.

Cd^{2+} binding studies suggested that His H126, His H128 and Asp H124 could function as a cluster constituting the unique entry point for protons from the bulk phase of the protein.[18,19] It has been proposed that protons taken up at this entry point would then be transferred to Q_B through a bifurcated pathway involving Asp M17 and Asp L210. This hypothesis was based on experiments combining Cd^{2+} binding effects on variants carrying respective replacements of Asp M17 and Asp L210 by Asn residues.[20] However, a different view can be derived from other results. We have performed the same kind of functional analysis on the L209PY RC variant in the presence of Cd^{2+}.[21] Identical effects on the electron and proton transfer kinetics were observed in this variant showing that the proton pathway from the bulk to Q_B does not only involve M17DN and L210DN *per se* but is likely to be more delocalized. In support of this hypothesis, we have previously shown that in the L212EA/L213DA double RC mutant, the pH dependencies of H^+/Q_A^- and H^+/Q_B^- proton uptake that collapse above pH 8 are remarkably restored to a WT level where an additional mutation (M249AY) is introduced in the close vicinity of Q_A.[22] The participation of a large

Figure 3. Proton translocating pathways. (a) the E-pathway is translocating protons from the bulk solvent, *via* Arg H118, and Asp M240 towards *Glu L212* and the vicinity of one methoxy-group of Q_B in the proximal position. (b) The D-pathway is translocating protons from the bulk solvent *via* Arg M13 towards *Asp L213* and the other methoxy-group of the proximal position of Q_B (italicised residues were used to name the pathways). An additional, flexible water molecule, invisible to the X-ray diffraction method, is probably necessary to translocate the proton to its actual destination, the oxo-group of Q_B. Molecules are drawn in licorice representation and possible hydrogen bonds are indicated by green broken lines, with their length given in Å. (c) Schematic drawing of the E-pathway and (d) of the D-pathway. Hydrogen atoms were added and oriented according to the acceptor and donor capabilities of neighboring hydrogen-bonded residues. The vertical water chain in the schematic drawings corresponds to the shortest connection through the water network of the pathways between Q_B in its proximal position and the bulk water. A flexible water molecule in red was added to either drawing to demonstrate a possible completion of the pathways at its Q_B end. To facilitate the identification of the water molecules forming the vertical water chain in (c) and (d), the possible H-bridges in (a) and (b) joining these water molecules of the chain, are indicated by orange, broken lines and their respective distance measures color-coded in red. All solvent molecules were given chain identifiers (id) in the respective PDB entry 2j8c, to indicate the protein chain to which they are most closely associated with: H subunit, solvent id S; M subunit, solvent id N; and L subunit, solvent id O. Xtalview[40] was used for visualization, Raster3D[60] for rendering, and ChemDraw for the schematic drawing.

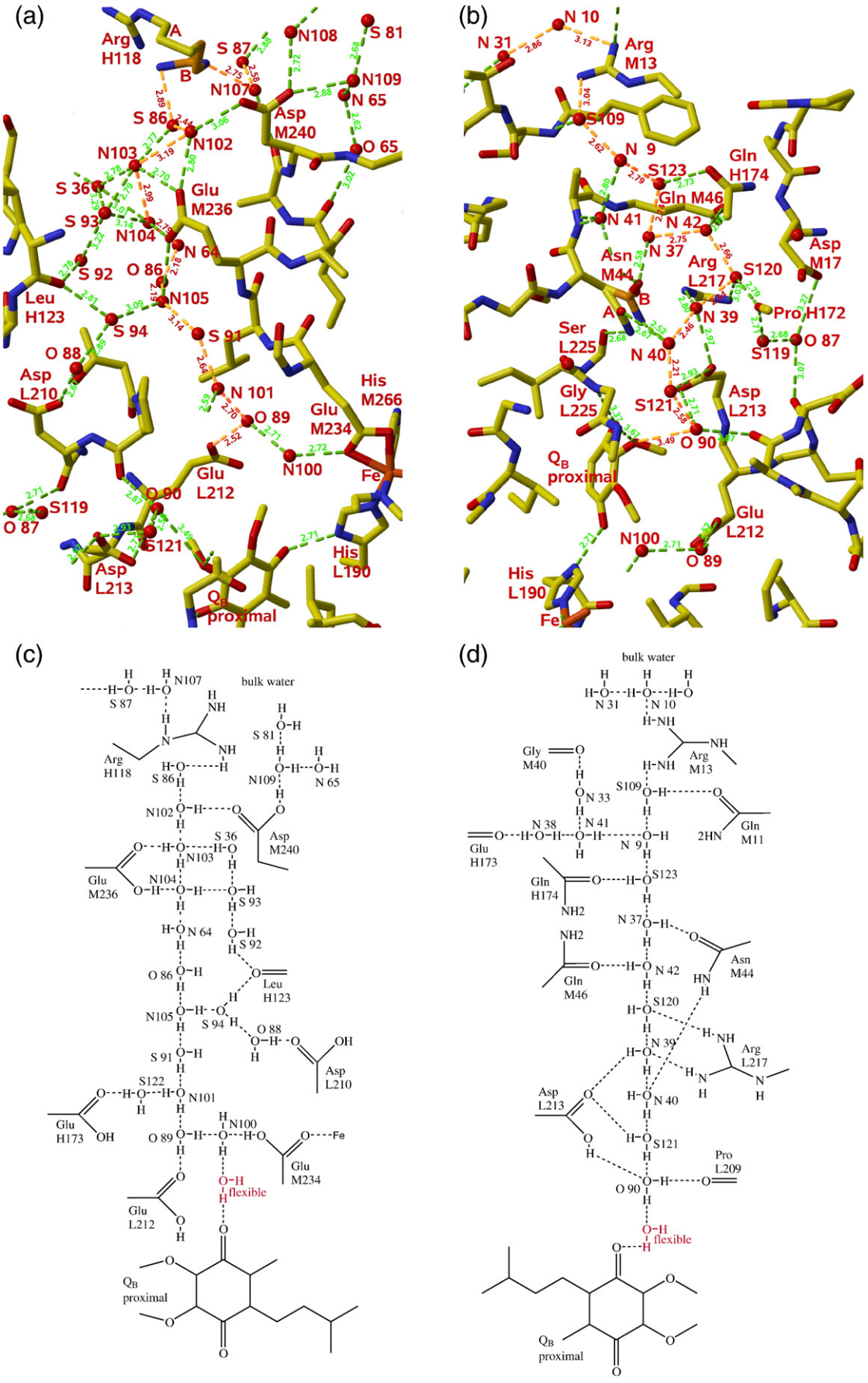

Figure 3 (*legend on previous page*)

portion of the inter-quinone cytoplasmic surface of the protein for taking up protons therefore seems to be more likely.

The present structural data demonstrating the existence of an extended proton transfer network starting at Arg H118 and Arg M13, which has never been reported before, support multiple entry points for protons as well as an extended proton transfer network within the protein to reach their target, the Q_B species.

Population of the two Q_B positions

The relative populations of the two Q_B positions in the dark-adapted and the illuminated state were calculated from the electron densities as described in Materials and Methods and are shown in Table 1. Due to a high correlation between temperature factors and occupancy of an atom in a medium resolution structure,[23] the occupancy could not be refined independently for the different Q_B positions (distal and proximal). However, assuming that the temperature factors are equal for the two positions, it is possible to estimate the relative populations for the two Q_B positions. The mean Q_B head-group temperature factors at the estimated populations are listed in Table 1. Test calculations indicate that only a small deviation in occupancy (0.1) can be compensated by an appropriate change in temperature factors at medium resolution.[24] Therefore we expect the error to be in the same range.

The computed population curves are shown in Figure 4. The population curve for Q_B in the dark-adapted state (Figure 4(a)) is in agreement with the experimentally determined data. There is only a slight pH dependence of the population. In order to track the possible origin of the variation of the Q_B population in the dark-adapted state, we have calculated the correlation function, c_{ip}, between the protonation of all titratable residues (i) and the proximal Q_B position (see Materials and Methods). By far the highest c_{ip} value arises from the interaction between Glu L212 (whose calculated protonation curve is presented in Figure 5(a)) and the Q_B proximal population. The c_{ip} correlation curve between the protonated Glu L212 and the proximal position of Q_B is presented in Figure 5(c). Obviously, the deprotonation of Glu L212 above pH 9 is correlated to the decrease of the proximal population (positive value of c_{ip}).

For the illuminated state, the computed populations (Figure 4(b)) coincide with the experimental data except for the experimental value measured at pH 6.5. However, the three evaluations of the proximal population for the illuminated state, respectively, 50, 50 and 60% arise from three independent measurements on three different crystals. Therefore these experimental points seem reliable.

Our model is satisfactory in fitting four dark (pH 6.5, 8.0, 9.0 and 10.0) and three illuminated states (pH 8.0, 9.0 and 10.0) based on the same structural information. The discrepancy between the calculated and measured populations for Q_B in the proximal position at pH 6.5 in the illuminated state may suggest that subtle structural changes may specifically occur at this pH that we cannot identify.

In a similar way as for the dark-adapted state we have probed the possible origin of the variation of the Q_B population in the illuminated state. We have also calculated the correlation function, c_{ip}, between the protonation of all titratable residues (i) and the proximal Q_B position (see Materials and Methods). Two protonable residues show high c_{ip} values. These are Asp L213 and Q_B itself, which calculated protonation curves are presented in Figure 5(b). The c_{ip} correlation curves between the protonated Asp L213 and the proximal position of Q_B, and between the protonated semiquinone and its proximal position are presented in Figure 5(d). Therefore, in the illuminated state, both the concomitant deprotonations of Asp L213 and the semiquinone lead to a decreased proximal population of Q_B^-.

An interesting feature displayed in Figure 5(d) is the very negative c_{ij} (see Materials and Methods) correlation curve between the protonated Asp L213 and the protonated semiquinone. The high calculated correlation c_{ij} reveals the strong destabilization of the proximal position for the deprotonated semiquinone when Asp L213 is deprotonated. Thus, according to our calculations the electrostatic repulsion between deprotonated Asp L213$^-$ and deprotonated Q_B^- depopulates the proximal position. When Q_B gets protonated, the proximal position can get more populated.

Proton uptake by Q_B and the complete RC

The proton uptake of the RC upon illumination was calculated as described in Materials and Methods. The computed proton uptake data in Figure 6 are similar to the experimental values,[25,26] although the shape of the experimental curve is not reproduced exactly. Between pH 4 and 8, Asp L213 and the ubiquinone (see below) almost exclusively account for the shape of the proton uptake curve. In contrast, in the pH range from 8 to 10, no individual residue could be identified that has a major influence on the proton uptake curve. Instead, many titratable groups contribute to the proton uptake in this pH range.

At low pH we find that the semiquinone is protonated predominantly (see Figure 5(b)). The protonation probability decreases slowly from a value of about 0.8 at pH 4.0 down to 0 at pH $\approx$ 9. In RCs isolated in detergent, the formation of Q_B^- leads to substoichiometric proton uptake in the pH range from 5 to 10.[25–28] At variance, it has been reported that in chromatophores from *Rb. capsulatus* and *Rb. sphaeroides* proton uptake occurs directly to the Q_B^- species to form a hydrosemiquinone (Q_BH) and leads to a measured value of $H^+/[RC]=1$ up a pH value of 7.[29] The Q_BH species deprotonates to Q_B^- in the pH range from 5 to 7. The titration curve observed by Lavergne *et al.*[29] has a much smaller slope than a standard Henderson-Hasselbalch curve would have. The calculated titration curve for the

Table 1. X-ray data collection statistics

pH	6.5					8.0		9.0			10.0			
Illumination	Dark	Light	Light	Dark	Light	Dark	Light	Dark	Light	Light	Dark	Light	Dark	Light
Accession code	2uww	2uws	2uwt	2uwu	2uwv	2j8c	2j8d	2ux3	2ux5	2ux4	2uxj	2uxk	2uxl	2uxm
Crystal	1	1	2	3	4	5	5	6	7	8	9	9	10	11
Q_B proximal occ. (%)	55	50	60	50	50	65	70	55	50	55	35	35	35	50
Q_B temp. factor (Å^2)	29.0	50.5	33.3	35.5	37.3	38.5	39.5	41.5	40.0	40.5	29.5	33.3	58.0	46.5
Space group			$P3_121$			$P3_121$			$P3_121$		$P4_32_12$		$P3_121$	
Unit cell parameters														
a (Å)	139.24	139.31	139.53	139.45	139.66	138.69	140.01	139.45	139.46	139.58	139.38	140.02	139.01	139.45
c (Å)	184.54	184.14	184.55	184.39	184.44	184.61	184.76	184.58	184.73	184.96	235.04	235.87	183.55	185.11
V (Å^3)	3,098,483	3,094,877	3,111,572	3,105,311	3,111,483	3,075,220	3,136,582	3,108,510	3,124,617	3,120,720	4,566,071	4,624,373	3,071,688	3,117,436
Resolution (Å)	2.05	2.9	2.5	2.04	2.13	1.87	2.07	2.5	2.21	2.5	2.25	2.31	2.85	2.7
Completeness (%)	99.7	93.2	98.0	98.0	98.8	87.0	95.6	92.1	93.3	97.8	93.9	93.8	81.3	94.3
R_{sym} (%)[a]	7.1	7.3	7.2	5.8	8.0	3.9	9.8	4.3	7.5	4.3	7.3	5.1	9.6	5.4
R_{free} (%)[b]	23.26	24.80	21.87	23.16	24.74	19.58	21.82	22.06	23.55	21.08	22.47	21.86	21.99	22.07
R (%)	20.47	20.20	19.55	20.78	22.54	17.82	19.73	18.54	20.20	18.96	19.37	18.99	17.58	18.56
Beamline		X11		X11		BW7B		BW7B	BW7B	X11	X11		PX	X11

[a] $R_{sym} = \Sigma_{hkl}\Sigma_i | I_i - \langle I \rangle | / \Sigma \langle I \rangle$, where I_i is the intensity of the *i*th measurement of reflection *hkl* and $\langle I \rangle$ is the average intensity of a reflection.
[b] R_{free} is calculated from 5% of the measured unique data that were not used during refinement.

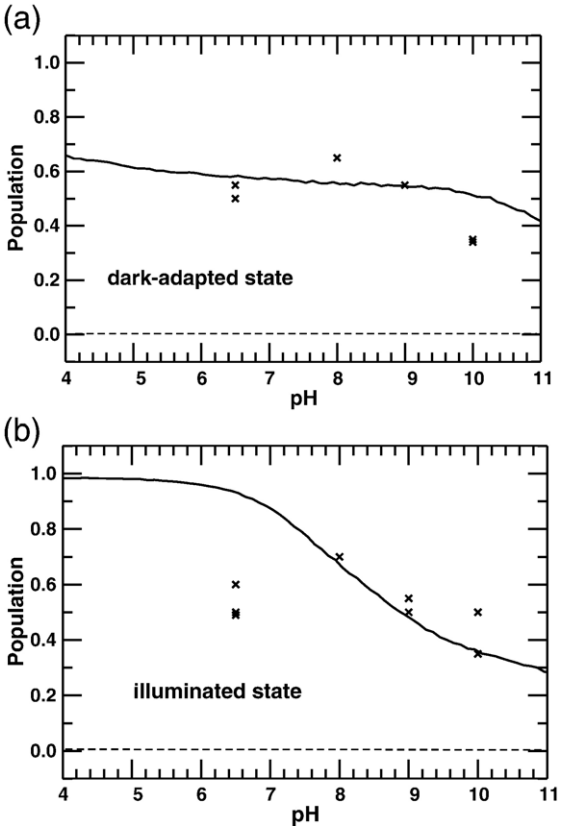

Figure 4. Calculated populations of the proximal bound Q_B in the dark-adapted (a) and in the illuminated state (b), respectively. The crosses depict the experimental values determined by the structure refinements performed in this work. Populations were calculated using the Monte Carlo program GMCT.

semiquinone shown in Figure 6 is reminiscent of the report by Lavergne *et al.*,[29] but with a more shallow shape. These authors have suggested that the apparent p*K* (~6) of the semiquinone form in chromatophores, would not reflect electrostatic interactions but would rather be due to a conformational change affecting the quinone binding and occurring between pH 5 and 7.

We do observe here an unexpected change in the quinone population at pH 6.5 in the illuminated state, which we cannot explain by our calculations. Our model is successful in fitting seven (four dark adapted state and three illuminated state pH points) out of eight quinone populations *versus* pH as determined by X-ray diffraction crystallography. However, we are unable to fit the point measured at pH 6.5 in the illuminated state. This point has been repeated three times (50, 50 and 60% proximal occupation) on three different samples. It is therefore quite firm. We are facing an apparent discrepancy between the measured position of the quinone in the illuminated state by crystallography and evaluated by electrostatic calculations.

The reason for this discrepancy will be further investigated.

Improvements to earlier calculations

Several theoretical studies on protonation probabilities and conformational changes of the Q_B binding site have been performed previously.[7,8,12,30–36] Apart from Taly *et al.*,[8] none of these studies considered the pH dependence of the population of the distal and proximal position.

The results of the calculations by Taly *et al.*[8] propose that with increasing pH the probability of the proximal conformation increases independently of whether the quinone or the semiquinone is bound. This finding was not confirmed by experimental data or by the calculations reported here.

An explanation for this discrepancy is that by Taly *et al.*,[8] the semiquinone was not considered as protonatable in the illuminated state. However, as shown in Figure 5(d), the protonation state of the semiquinone Q_B influences its own binding position. Neglecting this influence will therefore modify the calculated proximal population.

Moreover in our previous study,[8] we used two independently refined crystal structures as models for the proximal and the distal positions of Q_B. These two structures also differ in residues outside of the binding pocket. Here we used one structure for each state (dark-adapted and illuminated) to analyze the position of the quinone in which Q_B was modeled as a disordered residue. A detailed analysis of the correlation of our previous calculation[8] shows that residues outside of the Q_B binding pocket trigger the transition between the distal position found in the dark-adapted state and the proximal position found in the illuminated state. This behavior was an artefact of the approach. In the present study, this problem is avoided and the structural transition depends only on the protonation of residues in the vicinity of Q_B and of Q_B itself.

Conclusion

By X-ray diffraction crystallography, we have analyzed the binding position of the secondary quinone as a function of pH in the reaction center from *Rb. sphaeroides*. The different structures of the protein have been obtained at pH 6.5, 8.0, 9.0 and 10.0, in the dark adapted and illuminated states.

The electron density in the Q_B binding pocket, obtained with good quality data, suggests a new orientation of Q_B in the distal position, which has never been described before. In this conformation, no rotation of the head-group of Q_B is needed for its movement between the distal and the proximal positions. Most likely a putative movement between the distal and proximal binding of Q_B is not a rate-limiting factor for the Q_A^- to Q_B electron transfer.

We confirm the existence of two potential proton delivery pathways and further extend their content to new water molecules and residues close to the protein surface. These pathways can be involved in the proton delivery to the two oxo-groups of Q_B in the proximal position. It is interesting to note that

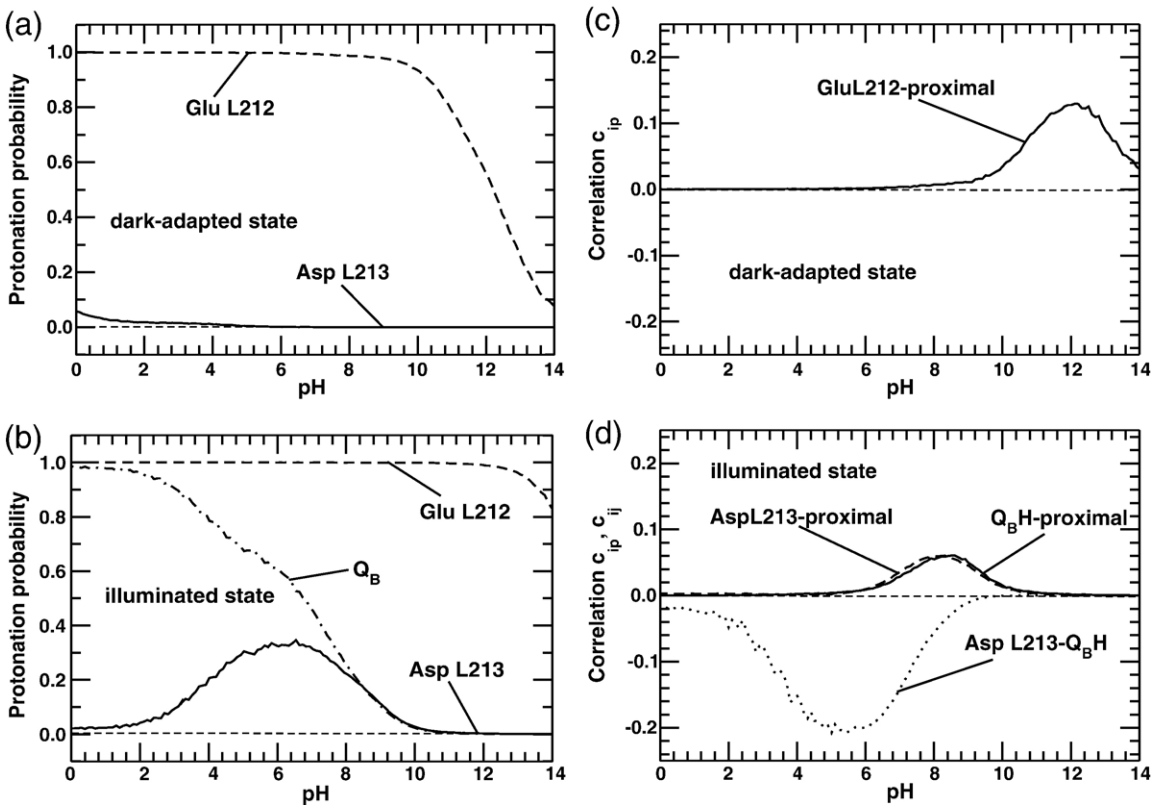

Figure 5. (a) Dark-adapted state: protonation probability of Glu L212 (broken line) and Asp L213 (continuous line). (b) Illuminated state: protonation probability of Q_B (dash-dot line). Same as in (a) for Glu L212 and Asp L213. (c) Dark-adapted state; calculated correlation, c_{ip} (see Materials and Methods for details) between the protonation of Glu L212 and the proximal position of Q_B (continuous line). (d) Illuminated state; correlation c_{ip} between the protonation of Q_B and the proronation of its proximal position (continuous line); c_{ip} between the protonation of Asp L213 and the proximal position of Q_B (broken line); correlation c_{ij} between the protonation of Q_B and Asp L213 (dotted line). Protonation probabilities and correlations were calculated using the Monte Carlo program GMCT.

these proton pathways start at Arg H118 and Arg M13, respectively. These entry points for protons are distinct from the previously proposed "unique" entry point formed by Asp H124, His H126, and His H128.[20] Our present finding further supports the previously suggested idea[21,22] that neither the proton entry points nor their pathways to the Q_B site are unique. Instead, the RC works more like a proton "trap" as previously described.[37] The higher the obtained resolution of the crystal structure, the more water molecules are detected and the more diverse potential proton transfer pathways are identified.

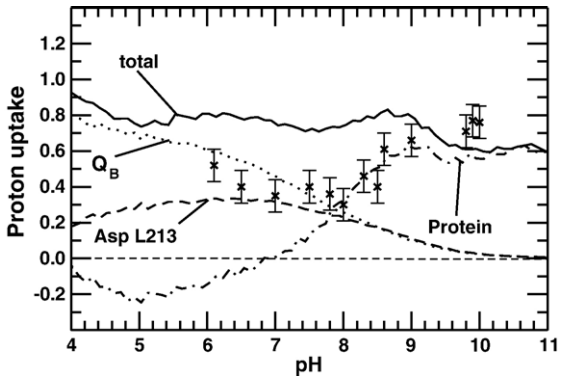

Figure 6. Proton-uptake upon reduction of Q_B as calculated using the program GMCT. The total proton-uptake is shown by a continuous line and experimental values (taken from Tandori *et al.*[22]) by black crosses with error bars. The contribution of Asp L213 (broken line) and the protonation of the semiquinone (dotted line) are shown additionally. The dash-dot line describes the proton uptake by the rest of the protein.

It is certainly a physiological advantage for the RC to transfer protons through several pathways. The alternative activation of these proton transfer pathways depends on the relative *p*Ks of their participating groups. Multiple proton transfer pathways have the advantage that a single mutation does not lead to the loss of function of the protein. In this regard, multiple pathways within the protein delivering protons certainly provide a higher functional flexibility and a higher evolutionary fitness.

As we show here, pH is important for positioning the quinone in its site and this positioning is correlated to the proton uptake. We were able to fit the pH dependencies of the quinone position and the proton uptake upon charge separation at the same time. Our results indicate that pH should be taken into account as a parameter regulating cofactor activities in proteins, for example by influencing their binding positions and/or affinities.

Materials and Methods

Crystallographic data collection and refinement

The RC from *Rb. sphaeroides* was purified and crystallized as reported earlier.[9] Reconstitution to obtain a fully occupied Q_B binding site, illumination conditions to achieve a complete charge separation, and stepwise equilibration with the cryo-buffer have been described previously.[2] The RCs crystallized in the space group $P3_121$, but occasionally in the same crystallization batch, tetragonal crystals of space group $P4_32_12$ were formed. We measured 14 datasets at four different pH values, 6.5, 8, 9, and 10 using 11 different crystals (Table 1). The first two pH 6.5 datasets and both pH 10 datasets with space group $P4_32_12$ were measured like both pH 8 datasets from the same crystal (crystals 1, 5, and 9 in Table 1). In other cases, the crystal did not survive the thawing and illumination after measuring the dark dataset. For some pH values, additional datasets were taken as control. In particular, illuminated datasets were repeated to ensure the illumination experiment had not failed. Except for one dataset, all data were collected at the beamlines X11 and BW7B of the EMBL-Outstation in Hamburg. The second dark dataset at pH 10 (crystal 10 in Table 1) was collected at the protein crystallographic (PX) beamline of the Swiss Light Source (SLS) in Villigen/CH.

When we refer here to a pH value in connection with an investigated dataset or a refined structure, we actually mean that the pH was adjusted by the potassium-hydrogen-phosphate buffer in each crystallization attempt. Since the pH value is defined as the negative logarithm of the chemical potential of the hydronium ions, which is constant in the whole system (solution and crystal) in thermodynamic equilibrium, this assignment is justified. Measured datasets were processed with the HKL program suite[38] and structure factors were calculated from the measured intensities employing TRUNCATE of the CCP4 (Collaborative Computing Project, 1994). Refinement was carried out using Refmac5.[39] The Q_B site is expected to be fully occupied, i.e. occupancies of the distal and the proximal positions add up to 100%. The populations of the two positions are thus equal to the occupancies, which are characterized by identical temperature factors for Q_B in the two positions.

Between each refinement round $2F_o–F_c$ and $F_o–F_c$ electron density maps were inspected using the graphics program XtalView.[40] Firmly bound water molecules were added by detecting peaks >3σ in the $F_o–F_c$ difference density map with a geometry suitable for hydrogen bonding. The quality of the electron density can be judged from Figure 1, where the electron density of 1.87 Å resolution around a refined cardiolipin (CDL), a GGD, and a PC molecule is shown. The molecules were found roughly at the same position as by Jones *et al.*[41] for the AM260W mutant (PDB entry 1qov) and by Camara-Artigas *et al.*[13] (PDB entry 1m3x). However, the orientation of the headgroup of the GGD molecule is pointing in the opposite direction (Figure 1(b)), while the PC molecule is rotated by about 70° (Figure 1(c)), thus placing them roughly parallel to the CDL molecule (Figure 1(d)). In this orientation, the PC is no longer in steric conflict with the isoprenoid tail of Q_B in the distal position (Figure 1(c)). Another example for the map quality can be inspected in Figure 2(a), where the electron density of the two Q_B positions (distal and proximal) in the Q_B binding pocket at pH 8 in the dark-adapted state is shown again with a resolution of 1.87 Å. In preliminary data collections, we were not able to detect any useful density in the Q_B binding pocket, indicating that the native Q_B must got lost during the purification procedure. However, we might not exclude an amount of native ubiquinone-10 remaining in the binding pocket unverifiable to X-ray diffraction methods. To replenish this loss, crystals were soaked with ubiquinone-2. The density found in the Q_B binding site after soaking was consequently modeled by a quinone with an isoprenoid-tail consisting of only two units. Therefore a similar density observed in the *Rps. viridis* reaction center[42] and modeled by a longer isoprenoid tail was refined in this work against a LDAO detergent molecule and three water molecules, in hydrogen bond distance to two LDAO head-group oxygen atoms in the periplasmic solvent region.

Structure preparation for theoretical calculations

The two crystal structures obtained for the dark-adapted and the illuminated state at pH 8 were used for the calculations. The electron density of the N and C termini of the H subunit (ten residues each) and the C terminus of the M subunit (five residues) was lacking in both structures. Since all of these three terminal regions have helical folds, the missing amino acids were used to elongate the respective helices. In a subsequent refinement round, very weak electron density showed up for some of the added amino acids. In each of the structures, the two possible binding positions of ubiquinone in the Q_B binding site are resolved. The hydrogen atoms were placed with the HBUILD module[43] of CHARMM[44] followed by an energy optimization of the hydrogen atom positions while the heavy-atom positions were kept fixed. The same partial charges were used as in previous calculations.[8,34,35,45] The detergent molecules seen in the crystal structures were taken into account explicitly.

The structures of the dark-adapted and illuminated RC were modified in loop regions (L, 149–165; M, 230–250; H, 137–165) in order to remove minor structural differences that cause a different titration behavior but were structurally insignificant. Therefore the coordinates of the named residues were taken from the higher resolved dark structure to replace the coordinates of the corresponding residues in the illuminated structure.

Protonation probability and population calculations

The pH-dependent protonation state energy $G^{n,l}(\mathrm{pH})$ of a certain protein conformation l and of a certain protonation state n is determined by the intrinsic pK ($\mathrm{p}K_a^{\mathrm{int},l}$) of each titratable group, the interaction energy W_{ij}^{l} between the charged forms of each possible pair of titratable groups and the conformational energy of the reference protonation state $\Delta G_{\mathrm{conf}}^{l}$:[46,47]

$$G_{n,l}(pH) = \sum_{i=1}^{N} \left(x_i^n - x_i^0\right) RT \ln 10 \left(pH - pK_{a,i}^{\mathrm{int},l}\right) + \frac{1}{2}\sum_{i=1}^{N}\sum_{j=1}^{N} W_{ij}^{l}\left(x_i^n - x_i^0\right)\left(x_j^n - x_j^0\right) + \Delta G_{\mathrm{conf}}^{l}$$

where x_i^0 is the reference protonation form and x_i^n the actual protonation form of the titratable group i. Both x_i^0 and x_i^n are 1 or 0 depending on whether the group is protonated or deprotonated. In the performed calculations, the reference protonation form of a titratable group is its neutral form (acidic groups 1; basic groups 0). The intrinsic pK is given by the experimentally determined pK ($\mathrm{p}K_{a,i}^{\mathrm{model}}$) of the titratable group alone in aqueous

solution[48] and the shift in the pK_a ($\Delta pK_{a,i}^{prot}$) due to a different solvation environment inside the protein ($pK_a^{int,l} = pK_{a,i}^{model} + \Delta pK_{a,i}^{prot}$). The terms $\Delta pK_{a,i}^{prot}$ and W_{ij}^{l} were calculated by solving the linearized Poisson-Boltzmann equation (LPBE) with the program package MEAD.[46] In the LPBE calculations, the effect of the solvent is modeled by a dielectric constant of 80 and an ionic strength of 0.1 mol/l. A dielectric constant of $\varepsilon = 4$ was assigned to the protein. A temperature of 300 K and the following atomic radii were used: 1.00 Å for hydrogen, 1.50 Å for oxygen, 1.55 Å for nitrogen, 1.70 Å for carbon and 1.80 Å for sulfur. The LPBE was solved by the finite difference method using three focusing steps for the protein and two for each titratable group: for the protein, the grid spacing was decreased from 2 Å to 1 Å and finally to 0.25 Å. For each titratable group, a grid spacing of 1 Å was used followed by a grid spacing of 0.25 Å. The boundary between the protein and solvent is defined by rolling a solvent probe sphere (radius 1.4 Å) over the van der Waals surface of the protein.[46]

In addition to the titratable groups of the amino acids of the protein, the semiquinone was considered as a titratable group. The model pK_a for all titratable residues are those reported earlier.[47] For the semiquinone a model pK_a of 4.9 was used.[49] For each titratable residue, the average protonation probability was calculated by a Monte Carlo procedure[50] using the program GMCT. All titratable residues were treated as a single tautomer (representing the average over all possible tautomers) except for histidine residues and semiquinone, for which two tautomers were included in the calculations. This treatment led to good agreement with experimental data in previous studies.[45,51–53]

In order to obtain the energy difference between the two possible orientations of Q_B in the distal position, we performed gas phase calculations on isolated Q_B using the Amsterdam Density Functional program suite[54] functionals VWN[55] and PW91.[56] Input coordinates of the two possible orientations of the distal Q_B positions were taken from our crystal structures at pH 8 and were subsequently minimized. We used the obtained relative gas phase energies together with results from electrostatic calculations to determine the probabilities of the two orientations of Q_B in the protein. The electrostatic calculations allow the protein to change its protonation states and were performed with MEAD (same parameters as above). GMCT was then used to perform the Monte Carlo titrations.

Analogously to the calculation of protonation probabilities, populations of the two Q_B positions were calculated using GMCT. Due to difficulties in determining ΔG_{conf}^{l} for the two positions by theoretical approaches,[52] this energy was adjusted to fit the experimental data points at pH 8.0 for the dark-adapted and illuminated states, respectively. This procedure is analogous to what we used previously.[8,52]

To analyze the mutual influence between the protonation forms of two given residues, we introduce[57,58] a correlation function, defined as: $c_{ij} = \langle x_i x_j \rangle - \langle x_i \rangle \langle x_j \rangle$, where $\langle x_i x_j \rangle$ is the probability of having residues i and j, both protonated at the same time and $\langle x_i \rangle$ and $\langle x_j \rangle$ are the respective probabilities of having residues i and j protonated independently.

To analyze the mutual influence between the protonation form of a given residue and the position of the Q_B, we also introduce a correlation function $c_{ip} = \langle x_i p \rangle - \langle x_i \rangle \langle p \rangle$, where $\langle x_i p \rangle$ is the probability that residue i is protonated when the Q_B is in the proximal position; $\langle p \rangle$ is the probability for Q_B to occupy the proximal position. $\langle p \rangle$ is equivalent to the proximal population.

c_{ij} and c_{ip} can vary in the range between −0.25 and +0.25. Positive values of the correlation functions correspond to mutual stabilisation of both events (protonation and/or proximal position). Negative values reflect destabilisation of one event (protonation or proximal position) by the other one.

The protonation probabilities of all titratable groups were computed for the dark-adapted and the illuminated state as described above. The resulting protonation probability difference between these two states corresponds to the number of protons taken up upon the first reduction of Q_B, which were compared with experimental data.[22,25]

Protein Data Bank accession codes

The continuum electrostatics calculations were based on the coordinates of the dark-adapted and illuminated 3D structures obtained at pH 8 and deposited together with their respective structure factors in the RCSB Protein Data Bank (PDB) with accession codes 2j8c and 2j8d, respectively. The different refined protein models and their respective structural amplitudes at the remaining pH values were deposited in the PDB as well. The corresponding accession codes of in the dark-adapted and illuminated states are at pH 6.5: 2uws to 2uww, at pH 9.0: 2ux3 to 2ux5, and at pH 10.0: 2uxj to 2uxm. In order to facilitate the assignment, the accession codes are also listed in Table 1.

Acknowledgements

We acknowledge help by the staff of the EMBL Hamburg Outstation and the European Community Access to Research Infrastructure Action of the Improving Human Potential Programme to the EMBL Hamburg Outstation, contract No. HPRI-CT-1999-00017. We thank Timm Essigke for his help with the electrostatic calculations. A. R. K. thanks Boehringer Ingelheim Fonds for a doctoral fellowship. This work was supported by the Max Planck Society and DFG grant UL174/7-1. We also thank the support of the German/French Procope bilateral travel grant no. 11438QH and D/0502198.

References

1. Stowell, M. H., McPhillips, T. M., Rees, D. C., Soltis, S. M., Abresch, E. & Feher, G. (1997). Light-induced structural changes in photosynthetic reaction center: implications for mechanism of electron-proton transfer. *Science*, **276**, 812–816.
2. Fritzsch, G., Koepke, J., Diem, R., Kuglstatter, A. & Baciou, L. (2002). Charge separation induces conformational changes in the photosynthetic reaction centre of purple bacteria. *Acta Crystallog. sect. D*, **58**, 1660–1663.
3. Graige, M. S., Paddock, M. L., Bruce, J. M., Feher, G. & Okamura, M. Y. (1996). Mechanism of proton-coupled electron transfer for quinone (QB) reduction in reaction centers of *Rb. sphaeroides*. *J. Am. Chem. Soc.* **118**, 9005–9016.
4. Graige, M. S., Paddock, M. L., Feher, G. & Okamura, M. Y. (1999). Observation of the protonated semiquinone intermediate in isolated reaction centers from *Rhodobacter sphaeroides*: implications for the mechanism of electron and proton transfer in proteins. *Biochemistry*, **38**, 11465–11473.

5. Breton, J., Boullais, C., Mioskowski, C., Sebban, P., Baciou, L. & Nabedryk, E. (2002). Vibrational spectroscopy favors a unique QB binding site at the proximal position in wild-type reaction centers and in the Pro-L209 –> Tyr mutant from *Rhodobacter sphaeroides*. *Biochemistry*, **41**, 12921–12927.
6. Xu, Q., Baciou, L., Sebban, P. & Gunner, M. R. (2002). Exploring the energy landscape for Q(A)(-) to Q(B) electron transfer in bacterial photosynthetic reaction centers: effect of substrate position and tail length on the conformational gating step. *Biochemistry*, **41**, 10021–10025.
7. Zachariae, U. & Lancaster, C. R. (2001). Proton uptake associated with the reduction of the primary quinone Q(A) influences the binding site of the secondary quinone Q(B) in *Rhodopseudomonas* viridis photosynthetic reaction centers. *Biochim. Biophys. Acta*, **1505**, 280–290.
8. Taly, A., Sebban, P., Smith, J. C. & Ullmann, G. M. (2003). The position of QB in the photosynthetic reaction center depends on pH: a theoretical analysis of the proton uptake upon QB reduction. *Biophys. J.* **84**, 2090–2098.
9. Ermler, U., Fritzsch, G., Buchanan, S. K. & Michel, H. (1994). Structure of the photosynthetic reaction centre from *Rhodobacter sphaeroides* at 2.65 Å resolution: cofactors and protein-cofactor interactions. *Structure*, **2**, 925–936.
10. Arnoux, B., Ducruix, A., Reiss-Husson, F., Lutz, M., Norris, J., Schiffer, M. & Chang, C. H. (1989). Structure of spheroidene in the photosynthetic reaction center from Y *Rhodobacter sphaeroides*. *FEBS Letters*, **258**, 47–50.
11. de Groot, H. J., Gebhard, R., van der Hoef, I., Hoff, A. J., Lugtenburg, J., Violette, C. A. & Frank, H. A. (1992). ^{13}C magic angle spinning NMR evidence for a 15,15′-cis configuration of the spheroidene in the *Rhodobacter sphaeroides* photosynthetic reaction center. *Biochemistry*, **31**, 12446–12450.
12. Lancaster, C. R. (1999). Quinone-binding sites in membrane proteins: what can we learn from the *Rhodopseudomonas* viridis reaction centre? *Biochem. Soc. Trans.* **27**, 591–596.
13. Camara-Artigas, A., Brune, D. & Allen, J. P. (2002). Interactions between lipids and bacterial reaction centers determined by protein crystallography. *Proc. Natl Acad. Sci. USA*, **99**, 11055–11060.
14. Fyfe, P. K. & Jones, M. R. (2005). Lipids in and around photosynthetic reaction centres. *Biochem. Soc. Trans.* **33**, 924–930.
15. Fritzsch, G., Kampmann, L., Kapaun, G. & Michel, H. (1998). Water clusters in the reaction centre of *Rhodobacter sphaeroides*. *Photosynth. Res.* **55**, 127–132.
16. Takahashi, E. & Wraight, C. A. (1990). A crucial role for AspL213 in the proton transfer pathway to the secondary quinone of reaction centers from *Rhodobacter sphaeroides*. *Biochim. Biophys. Acta*, **1020**, 107–111.
17. Paddock, M. L., Rongey, S. H., Feher, G. & Okamura, M. Y. (1989). Pathway of proton transfer in bacterial reaction centers: replacement of glutamic acid 212 in the L subunit by glutamine inhibits quinone (secondary acceptor) turnover. *Proc. Natl Acad. Sci. USA*, **86**, 6602–6606.
18. Axelrod, H. L., Abresch, E. C., Paddock, M. L., Okamura, M. Y. & Feher, G. (2000). Determination of the binding sites of the proton transfer inhibitors Cd2+ and Zn2+ in bacterial reaction centers. *Proc. Natl Acad. Sci. USA*, **97**, 1542–1547.
19. Paddock, M. L., Graige, M. S., Feher, G. & Okamura, M. Y. (1999). Identification of the proton pathway in bacterial reaction centers: inhibition of proton transfer by binding of Zn2+ or Cd2+. *Proc. Natl Acad. Sci. USA*, **96**, 6183–6188.
20. Paddock, M. L., Feher, G. & Okamura, M. Y. (2000). Identification of the proton pathway in bacterial reaction centers: replacement of Asp-M17 and Asp-L210 with asn reduces the proton transfer rate in the presence of Cd2+. *Proc. Natl Acad. Sci. USA*, **97**, 1548–1553.
21. Gerencser, L., Taly, A., Baciou, L., Maroti, P. & Sebban, P. (2002). Effect of binding of Cd2+ on bacterial reaction center mutants: proton-transfer uses interdependent pathways. *Biochemistry*, **41**, 9132–9138.
22. Tandori, J., Baciou, L., Alexov, E., Maroti, P., Schiffer, M., Hanson, D. K. & Sebban, P. (2001). Revealing the involvement of extended hydrogen bond networks in the cooperative function between distant sites in bacterial reaction centers. *J. Biol. Chem.* **276**, 45513–45515.
23. Kundrot, C. E. & Richards, F. M. (1987). Use of the occupancy factor in the refinement of solvent molecules in protein crystal structures. *Acta Crystallog. sect. B*, **43**, 544–547.
24. Bath, T. H. (1989). Correlation between occupancy and temperature factors of solvent molecules in crystal structures of proteins. *Acta Crystallog. sect. A*, **45**, 145–146.
25. McPherson, P. H., Okamura, M. Y. & Feher, G. (1988). Light-induced proton uptake by photosynthetic reaction centers from *Rhodobacter sphaeroides* R-26. I. Protonation of the one-electron states $D^+Q_A^-$, $D^+Q_AQ_B^-$ and $DQ_AQ_B^-$. *Biochim. Biophys. Acta*, **934**, 348–368.
26. Tandori, J., Maroti, P., Alexov, E., Sebban, P. & Baciou, L. (2002). Key role of proline L209 in connecting the distant quinone pockets in the reaction center of *Rhodobacter sphaeroides*. *Proc. Natl Acad. Sci. USA*, **99**, 6702–6706.
27. Maroti, P. & Wraight, C. A. (1988). Flash-induced H+ binding by bacterial photosynthetic reaction centers: influences of the redox states of the acceptor quinones and primary donor. *Biochim. Biophys. Acta*, **934**, 329–347.
28. Miksovska, J., Maróti, P., Tandori, J., Schiffer, M., Hanson, D. K. & Sebban, P. (1996). Distant electrostatic interactions modulate the free energy level of QA- in the photosynthetic reaction center. *Biochemistry*, **35**, 15411–15417.
29. Lavergne, J., Matthews, C. & Ginet, N. (1999). Electron and proton transfer on the acceptor side of the reaction center in chromatophores of *Rhodobacter capsulatus*: evidence for direct protonation of the semiquinone state of QB. *Biochemistry*, **38**, 4542–4552.
30. Alexov, E., Miksovska, J., Baciou, L., Schiffer, M., Hanson, D. K., Sebban, P. & Gunner, M. R. (2000). Modeling the effects of mutations on the free energy of the first electron transfer from QA- to QB in photosynthetic reaction centers. *Biochemistry*, **39**, 5940–5952.
31. Alexov, E. G. & Gunner, M. R. (1999). Calculated protein and proton motions coupled to electron transfer: electron transfer from QA- to QB in bacterial photosynthetic reaction centers. *Biochemistry*, **38**, 8253–8270.
32. Grafton, A. K. & Wheeler, R. A. (1999). Amino acid protonation states determine binding sites of the secondary ubiquinone and its anion in the *Rhodobacter sphaeroides* photosynthetic reaction center. *J. Phys. Chem. B*, **103**, 5380–5387.
33. Ishikita, H. & Knapp, E. W. (2004). Variation of Ser-L223 hydrogen bonding with the QB redox state in

reaction centers from *Rhodobacter sphaeroides*. *J. Am. Chem. Soc.* **126**, 8059–8064.
34. Rabenstein, B., Ullmann, G. M. & Knapp, E. W. (1998). Calculation of protonation patterns in proteins with structural relaxation and molecular ensembles-application to the photosynthetic reaction center. *Eur. Biophys. J.* **27**, 626–637.
35. Rabenstein, B., Ullmann, G. M. & Knapp, E. W. (2000). Electron transfer between the quinones in the photosynthetic reaction center and its coupling to conformational changes. *Biochemistry*, **39**, 10487–10496.
36. Walden, S. E. & Wheeler, R. A. (2002). Protein conformational gate controlling site preference and migration for ubiquinone B in the phtotosynthetic reaction center of *Rhodobacter sphaeroides*. *J. Phys. Chem. B*, **106**, 3001–3006.
37. Cheap, H., Tandori, J., Derrien, V., Benoit, M., de Oliveira, P., & Koepke, J. (2007). Evidence for delocalized anticooperative flash induced proton binding as revealed by mutants at the M266His iron ligand in bacterial reaction centers. *Biochemistry*, **46**, 4510–4521.
38. Otwinowski, Z. & Minor, W. (1997). Processing of X-ray diffraction data collected in oscillation mode. *Methods Enzymol.* **276**, 307–326.
39. Murshudov, G. N., Vagin, A. A., Lebedev, A., Wilson, K. S. & Dodson, E. J. (1999). Efficient anisotropic refinement of macromolecular structures using FFT. *Acta Crystallog. sect. D*, **55**, 247–255.
40. McRee, D. E. (1999). *Practical Protein Crystallography,* Academic Press.
41. Jones, M. R., Fyfe, P. K., Roszak, A. W., Isaacs, N. W. & Cogdell, R. J. (2002). Protein-lipid interactions in the purple bacterial reaction centre. *Biochim. Biophys. Acta*, **1565**, 206–214.
42. Lancaster, C. R. & Michel, H. (1997). The coupling of light-induced electron transfer and proton uptake as derived from crystal structures of reaction centres from *Rhodopseudomonas* viridis modified at the binding site of the secondary quinone, QB. *Structure*, **5**, 1339–1359.
43. Brunger, A. T. & Karplus, M. (1988). Polar hydrogen positions in proteins: empirical energy placement and neutron diffraction comparison. *Proteins: Struct. Funct. Genet.* **4**, 148–156.
44. Brooks, B. R., Bruccoleri, B., Olafson, D., States, D., Swaminathan, S. & Karplus, M. (1983). CHARMM: a program for macromolecular energy, minimization and dynamics calculations. *J. Comput. Chem.* **4**, 187–217.
45. Rabenstein, B., Ullmann, G. M. & Knapp, E. W. (1998). Energetics of electron-transfer and protonation reactions of the quinones in the photosynthetic reaction center of *Rhodopseudomonas* viridis. *Biochemistry*, **37**, 2488–2495.
46. Bashford, D. & Gerwert, K. (1992). Electrostatic calculations of the pK_a values of ionizable groups in bacteriorhodopsin. *J. Mol. Biol.* **224**, 4734–4786.
47. Ullmann, G. M. & Knapp, E. W. (1999). Electrostatic models for computing protonation and redox equilibria in proteins. *Eur. Biophys. J.* **28**, 533–551.
48. Tanford, C. & Roxby, R. (1972). Interpretation of protein probability curves. Application to lysozyme. *Biochemistry*, **11**, 2192–2198.
49. Morrison, L. E., Shelhorn, J. E., Cotton, T. E., Bering, C. L. & Loach, P. A. (1982). Electrochemical and spectral properties of ubiquinone and synthetic analogs: relevance to bacterial photosynthesis. In *Function of Quinones in Energy Conserving Systems* (Trumpover, B. L., ed.), pp. 35–38, Academic Press Inc.
50. Beroza, P., Fredkin, D. R., Okamura, M. Y. & Feher, G. (1991). Protonation of interacting residues in a protein by a Monte Carlo method: application to lysozyme and the photosynthetic reaction center of *Rhodobacter sphaeroides*. *Proc. Natl Acad. Sci. USA*, **88**, 5804–5808.
51. Bashford, D., Case, D. A., Dalvit, C., Tennat, L. & Wright, P. E. (1993). Electrostatic calculations of side-chain p*Ka* values in myoglobin and comparison with NMR data for histidines. *Biochemistry*, **32**, 8045–8056.
52. Rabenstein, B. & Knapp, E. W. (2001). Calculated pH-dependent population and protonation of carbon-monoxy-myoglobin conformers. *Biophys. J.* **80**, 1141–1150.
53. Ullmann, G. M. (2000). The coupling of protonation and reduction in proteins with multiple redox centers. Theory, computational method and application to cytochrome c3. *J. Phys. Chem. B*, **104**, 6293–6303.
54. te Velde, G., Bickelhaupt, F. M., Baerends, E. J., Guerra, C. F., van Gisbergen, S. J. A., Snijder, J. G. & Ziegler, T. (2001). Chemistry with ADF. *J.Comput. Chem.* **22**, 931–967.
55. Vosko, S. H., Wilk, L. & Nusair, M. (1980). Determining atom-centered monopoles from molecular electrostatic potentials. The need for high spin sampling density in formaide conformational analysis. *J. Comput. Chem.* **11**, 361–373.
56. Perdrew, J. P., Chevary, J. A., Vosko, S. H., Jacson, K. A., Pederson, M. R., Singh, D. J. & Fiolais, C. (1992). Atoms, molecules, solids and surfaces: applications of the generalized gradient approximation for exchange and correlation. *Phys. Rev. B*, **15**, 6671–6687.
57. Calimet, N. & Ullmann, G. M. (2004). The influence of a transmembrane pH gradient on protonation probabilities of bacteriorhodopsin: the structural basis of the back-pressure effect. *J. Mol. Biol.* **339**, 571–589.
58. Klingen, A. R., Palsdottir, H., Hunte, C. & Ullmann, G. M. (2007). Redox-linked protonation state changes in cytochrome bc1 identified by Poisson-Boltzmann electrostatics calculations. *Biochim. Biophys. Acta*, **1767**, 204–221.
59. Humphrey, W., Dalke, A. & Schulten, K. (1996). VMD: visual molecular dynamics. *J. Mol. Graph.* **14**, 33–38.
60. Merritt, E. A. & Bacon, D. J. (1997). Raster 3D: photorealistic molecular graphics. *Methods Enzymol.* **277**, 505–524.

Edited by R. Huber

(Received 16 November 2006; received in revised form 5 April 2007; accepted 17 April 2007)
Available online 10 May 2007